An acetylated form of histone H2A.Z regulates chromosome architecture in *Schizosaccharomyces pombe*

Hyun-Soo Kim[1,10], Vincent Vanoosthuyse[2,10], Jeffrey Fillingham[3], Assen Roguev[4,5], Stephen Watt[6], Thomas Kislinger[7], Alex Treyer[1], Laura Rocco Carpenter[8], Christopher S Bennett[8], Andrew Emili[3,9], Jack F Greenblatt[3,9], Kevin G Hardwick[2], Nevan J Krogan[4,5], Jürg Bähler[6] & Michael-Christopher Keogh[1]

Histone variant H2A.Z has a conserved role in genome stability, although it remains unclear how this is mediated. Here we demonstrate that the fission yeast Swr1 ATPase inserts H2A.Z (Pht1) into chromatin and Kat5 acetyltransferase (Mst1) acetylates it. Deletion or an unacetylatable mutation of Pht1 leads to genome instability, primarily caused by chromosome entanglement and breakage at anaphase. This leads to the loss of telomere-proximal markers, though telomere protection and repeat length are unaffected by the absence of Pht1. Strikingly, the chromosome entanglement in *pht1Δ* anaphase cells can be rescued by forcing chromosome condensation before anaphase onset. We show that the condensin complex, required for the maintenance of anaphase chromosome condensation, prematurely dissociates from chromatin in the absence of Pht1. This and other findings suggest an important role for H2A.Z in the architecture of anaphase chromosomes.

The basic repeating unit of chromatin is the nucleosome core particle: 146 base pairs (bp) of DNA wrapped around a core histone octamer composed of a $(H3-H4)_2$ tetramer and two H2A-H2B dimers. One means of nucleosome specialization is the replacement of a major histone with a specific variant. These single-copy nonallelic isoforms are generally expressed throughout the cell cycle, and many enter nucleosomes through the action of specific deposition machineries[1]. Both major and variant histones can be further distinguished by the addition of small chemical moieties, including phosphorylation, acetylation, methylation and ubiquitylation[2,3].

H2A.Z is one of the most-studied histone variants. In metazoans H2A.Z is essential[4], regulating chromosome stability[5], gene activation[6,7] and spermatogenesis[8]. The histone is subject to multiple N-terminal acetylations in *Saccharomyces cerevisiae* (*Sc*)[9–11], *Tetrahymena thermophila*[12] and metazoans[13,14]. Though the role(s) of these modifications remains uncertain, defects in heterochomatin restriction[11] and chromosome stability[9] are observed when unacetylatable H2A.Z alleles are expressed as the sole source of the histone in budding yeast.

A phenotype common to all H2A.Z-deficient species is genomic instability. This manifests in mammalian cells as chromatin bridges in anaphase[5]. Deletion of *Sc* H2A.Z (*htz1Δ*) results in an increased rate of chromosome loss, sensitivity to microtubule destabilizing agents, and synthetic genetic interactions with components of the kinetochore and spindle checkpoint machineries[15]. Many of these phenotypes are shared by an unacetylatable *htz1* mutant, suggesting a role for acetylation in genomic stability[9]. However, we still have

little mechanistic understanding of what leads to the chromosome segregation defect in these cells, though centromere organization, kinetochore attachment, cohesin recruitment and arm sister chromatid cohesion appear normal[9].

To explain the role of H2A.Z in chromosome stability, we turned to the fission yeast *Schizosaccharomyces pombe* (*Sp*) as its three large chromosomes (3×3.5–5.7 Mb) can be more easily monitored during mitosis than those of budding yeast (16×230 kb–1.3 Mb). We show that *Sp* H2A.Z (pseudohistone 1, or Pht1) copurifies with a complex almost identical in composition to the *Sc* SWR complex (SWR-C, with this complex required for the insertion of Pht1 into chromatin. Chromatin-associated Pht1 is acetylated on its N terminus by the KAT5 acetyltransferase (*Sp* Mst1). This modification is essential for Pht1 function, with unacetylatable mutants phenocopying complete deletion of the histone variant in all analyses, including genome-scale genetic interaction and gene expression studies. In addition, we show that chromosome loss in *pht1* mutants is primarily caused by broad architectural defects and can be suppressed by improving chromosome condensation. Consistent with this, we show by chromatin immunoprecipitation that the condensin complex is prematurely released from chromatin at anaphase in *pht1Δ* cells.

RESULTS

Pht1 is acetylated as a component of chromatin

Sp Pht1 has four potentially acetylatable lysine residues on its N terminus: Lys5, Lys7, Lys12 and Lys16 (**Fig. 1a**). We synthesized

[1]Department of Cell Biology, Albert Einstein College of Medicine, New York, New York, USA. [2]Wellcome Trust Centre for Cell Biology, University of Edinburgh, Edinburgh, Scotland, UK. [3]Banting and Best Department of Medical Research, University of Toronto, Toronto, Canada. [4]Department of Cellular and Molecular Pharmacology and [5]The California Institute for Quantitative Biomedical Research, University of California–San Francisco, San Francisco, California, USA. [6]Wellcome Trust Sanger Institute, Cambridge, UK. [7]Ontario Cancer Institute, Toronto, Canada. [8]Active Motif Inc., Lake Placid, New York, USA. [9]Department of Molecular and Medical Genetics, University of Toronto, Toronto, Canada. [10]These authors contributed equally to this work. Correspondence should be addressed to V.V. (vvanoost@staffmail.ed.ac.uk) or M.-C.K. (michael.keogh@einstein.yu.edu).

Figure 1 Chromatin-associated Pht1 is acetylated by Mst1. (**a**) Alignment of the H2A.Z N termini from *Sc* (Htz1, YOL012C), *Sp* (Pht1, SPBC11B10.10c), *Drosophila melanogaster* (*Dm*; H2Av, P028985), *Mus musculus* (*Mm*; NP_058030) and *Homo sapiens* (*Hs*; NP_002097). Pht1 is misannotated in the literature by the addition of 32 N-terminal residues (MILRHAPRVHESAFSLTHKTFAFCNCNNRFKM-). This would give a protein of 18 kDa rather than the 14 kDa observed. The acetylated residues on *Sc* Htz1 (Lys3, Lys8, Lys10 and Lys14) correspond to *Sp* Pht1 Lys5, Lys7, Lys12 and Lys16. A synthetic tetra-acetylated peptide covering this region (boxed) was injected into rabbits to create anti-Pht1^{Ac}. (**b**) Pht1 is acetylated on the N terminus. Immunoblotting was performed on strains expressing C-terminally HA$_3$-tagged Pht1 (or indicated mutants) at the endogenous locus. Total Pht1 was detected by anti-HA (12CA5; **Supplementary Table 3**). * in anti-Pht1^{Ac} panel refers to cross-reaction with H4ac. H3 and Rpn8 serve as loading controls. (**c**) The *mst1-L271P* allele is slow and *ts*. Spot tests are ten-fold dilutions onto YES plates. (**d**) WCEs from *mst1-L271P* show a profound reduction in Pht1^{Ac} without affecting total Pht1 or H3ac levels. H3 and Rpn8 serve as loading controls. (**e,f**) Pht1 acetylation by Mst1 is not required for assembly of the histone into chromatin. In **f**, strains express Pht1.HA$_3$ or unacetylatable *pht1-4KQ*.HA$_3$ at the endogenous locus. Cells were treated to form (Total, Tot) and fractionated into cytoplasm (Cyt), nucleus (Nuc) and chromatin (Chr). H3 and Rpn8 controls (*cross-reacting species) indicate efficient fractionation: the former is primarily localized in insoluble chromatin, the latter in soluble cytoplasm.
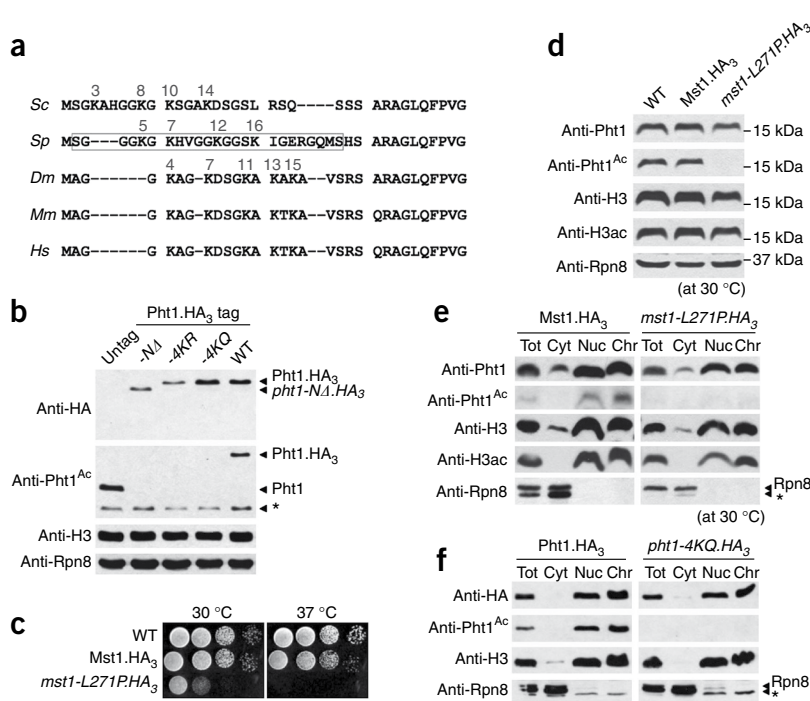
a peptide containing all four acetyllysines and immunized rabbits to create polyclonal anti-Pht1^{Ac}. On immunoblots of *Sp* whole cell extracts (WCEs) this antibody recognized a protein of appropriate size for Pht1. This signal disappears in WCEs from *pht1Δ, -NΔ* (deletion of the N terminus), or mutants where all four lysines were mutated to unacetylatable arginine or glutamine (**Fig. 1b**). Thus, the Pht1 N terminus is acetylated and we have a specific reagent for the modification.

The primary acetyltransferase for *Sc* Htz1 is Esa1, the catalytic subunit of the NuA4 complex[9–11]. Esa1 is a member of the KAT5 family, with the most likely *Sp* homolog the essential protein Mst1 (ref. 16). We created a temperature-sensitive (*ts*) allele of Mst1 (*mst1-L271P*) that resulted in slow growth at the permissive temperature (25 °C) and was lethal at >34 °C (**Fig. 1c**). WCEs from *mst1-L271P* cells showed no appreciable change in total Pht1 levels but did show a profound reduction in Pht1^{Ac} (**Fig. 1d**), indicating that Pht1 acetylation is Mst1 dependent. Cell fractionation showed that Pht1^{Ac} is chromatin associated, though acetylation is not required for entry to this cellular compartment (**Figs. 1e–f**).

Sc Htz1 associates with the SWR-C, containing the Swr1 ATPase, and incorporation of the histone into chromatin is markedly reduced in *swr1Δ* cells[17–19]. We subjected WCEs from Pht1.TAP to sequential affinity purification and identified the associated proteins by MS (**Supplementary Table 1**). Reciprocal tagging and purification of these factors delineates the *Sp* SWR-C, which is almost identical in composition to the *Sc* SWR-C: even the subunits shared between the *Sp* SWR-C and the Mst1-acetyltransferase complex are those shared by their *Sc* counterparts, the SWR-C and NuA4 (**Fig. 2a**). Western analysis with anti-Pht1^{Ac} distinguished those subunits of the *Sp* SWR-C required for the efficient acetylation of the histone (**Fig. 2b**), most

likely because of inefficient assembly of the variant into chromatin in each background (**Fig. 2c**). Thus, a pathway first identified in *Sc* also operates in *Sp*: SWR-C inserts Pht1 into chromatin, where it is acetylated by Mst1.

Acetylation is integral to Pht1 function

To determine the relevance of N-terminal acetylation to Pht1 function, we compared the gene expression and genetic interaction profiles of various unacetylatable mutant alleles (*pht1-NΔ, -4KR,* and *-4KQ*) to *pht1Δ*. The transcription profiles of the unacetylatable mutants were almost identical to those of *pht1Δ* (for example, relative *P* value: Δ to *-4KR* = 2e^{-195}; **Fig. 3a**). A noteworthy observation was that almost all genes were modulated to some degree in *pht1* mutants (**Fig. 3b**), suggesting that the histone acts as a general transcriptional regulator. By comparison, *swr1Δ* showed weaker changes in gene expression (**Fig. 3b**). As loss of the ATPase strongly reduces but does not completely ablate chromatin-associated Pht1 (**Fig. 2c**), it is likely that the remaining Pht1 is sufficient to mask most H2A.Z-dependent phenotypes.

We then used the Pombe Epistatic Mapper 2 (PEM-2) system to quantitatively analyze genetic interaction patterns[20,21]. To this end we individually crossed *pht1Δ, -NΔ, -4KR, -4KQ* and *swr1Δ* strains to a library of 2,161 nonessential *Sp* deletions (the Bioneer collection) and derived scores covering each negative (for example, synthetic sick or lethal) and positive (for example, suppression) genetic interaction using colony size as a quantitative readout[20,22–24]. Positive interactions enrich for factors that are in complex together or function in the same pathway[20,22,23]. Consistent with this, *pht1Δ*, unacetylatable *pht1* and *swr1Δ* each gave rise to positive genetic interactions in combination with deletion of all nonessential subunits of the SWR-C[20] (**Fig. 3c**).
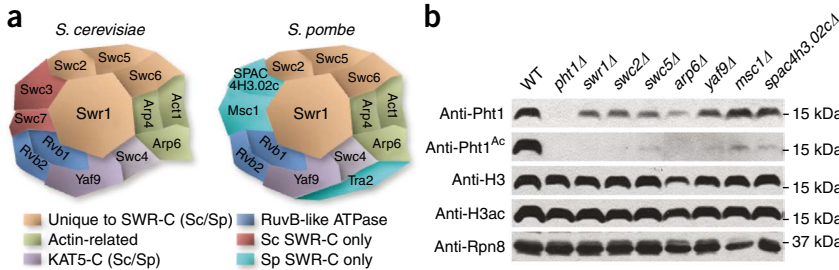
Figure 2 Pht1 is inserted into chromatin by the SWR-C. (**a**) The SWR-C is highly conserved from *Sp* to *Sc*. Multiple subunits of each complex were C-terminally tagged for TAP and associated factors identified by MS[17] (**Supplementary Table 1**). In this schematic, location does not indicate direct interaction. (**b**) SWR-C components are individually required for the efficient acetylation of Pht1, suggesting chromatin-insertion defects. Total Pht1 levels are also reduced in many of these mutants. Immunoblotting of H3, H3ac and Rpn8 serve as loading controls. (**c**) Pht1 is inefficiently assembled into chromatin in *swr1Δ*, and to a lesser extent in *msc1Δ*. Schematic depicts the neighborhood of constitutively expressed *adh1+*. Black boxes depict the location of ChIP primers (**Supplementary Table 5**) relative to the start codon (+1). Pht1.HA$_3$ was detected by anti-HA. Appropriate localization of Tbp1 at the *adh1+* promoter confirms sample integrity. In these duplex reactions, upper band (*adh1* locus) is the specific primers numbered in the schematic; lower band is a nontranscribed gene-free region (GFR) included as a loading control. Lower panel (Input) is used to normalize the PCR amplification efficiency of each primer pair.
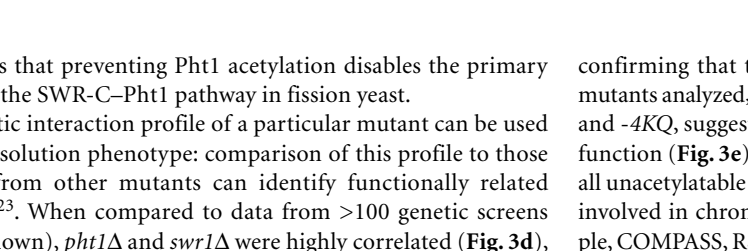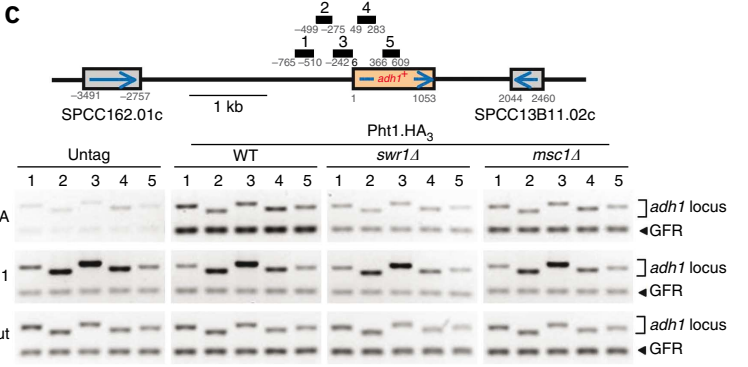
This implies that preventing Pht1 acetylation disables the primary function of the SWR-C–Pht1 pathway in fission yeast.

The genetic interaction profile of a particular mutant can be used as a high-resolution phenotype: comparison of this profile to those generated from other mutants can identify functionally related factors[20,22,23]. When compared to data from >100 genetic screens (data not shown), *pht1Δ* and *swr1Δ* were highly correlated (**Fig. 3d**),

confirming that they function in the same pathway. Indeed, of all mutants analyzed, the most highly correlated to *pht1Δ* were *-NΔ, -4KR* and *-4KQ*, suggesting that N-terminal acetylation is critical for Pht1 function (**Fig. 3e**). Inspection of individual interactions showed that all unacetylatable *pht1* alleles were synthetic, with deletions of factors involved in chromatin modification and/or remodeling (for example, COMPASS, RSC, SET3-C), transcription (for example, Mediator)
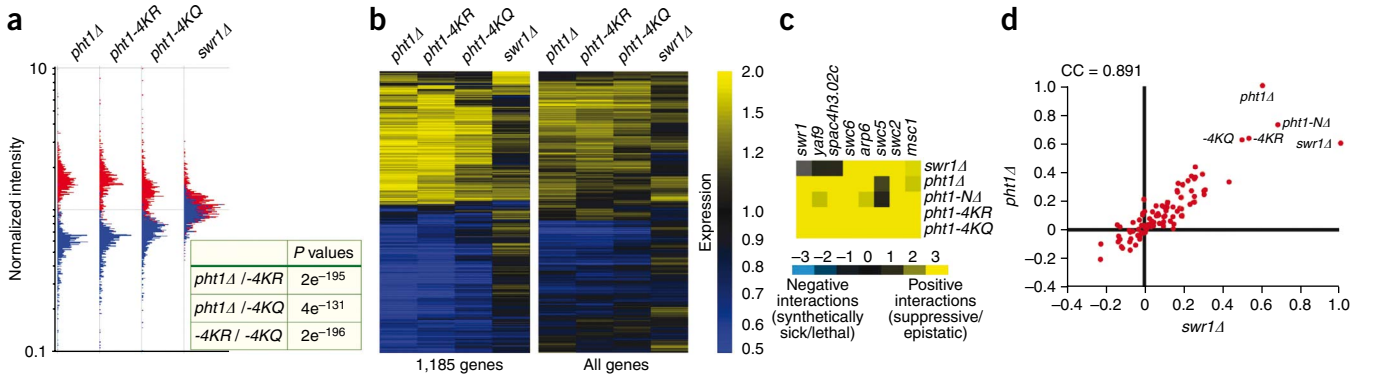
Figure 3 Unacetylatable *pht1* mutants phenocopy *pht1Δ*. (**a**) Panel compares genes whose expression is induced (red) and repressed (blue) (by a factor of at least 1.5 in at least one condition) as indicated by whole-genome array data from each strain. Relative *P* values for expression overlaps among induced genes between strain pairs are as indicated. (**b**) Heat map of induced (yellow) and repressed (blue) genes in each mutant. Left, 1,185 genes are changed by a factor of at least 1.5 in at least one mutant background. Right: all genes on the array. (**c**) Unacetylatable *pht1* mutants display positive genetic interactions with deletions of SWR-C subunits. (**d**) Correlation coefficient (CC) plot comparing the genetic interactions of 101 query mutants (including *pht1Δ, -NΔ, -4KR, -KQ* and *swr1Δ*) mated against a library of 2,161 nonessential deletions. Red dots indicate the CC of each genetic screen to the mutants on the *x* or *y* axis. (**e**) CC plot of *pht1Δ* versus *pht1-4KQ*. (**f**) *pht1Δ, -NΔ, -4KR, -KQ* and *swr1Δ* share a large number of synthetic genetic interactions, including with members of the COMPASS, RSC, SET3-C, Mediator and DASH complexes.
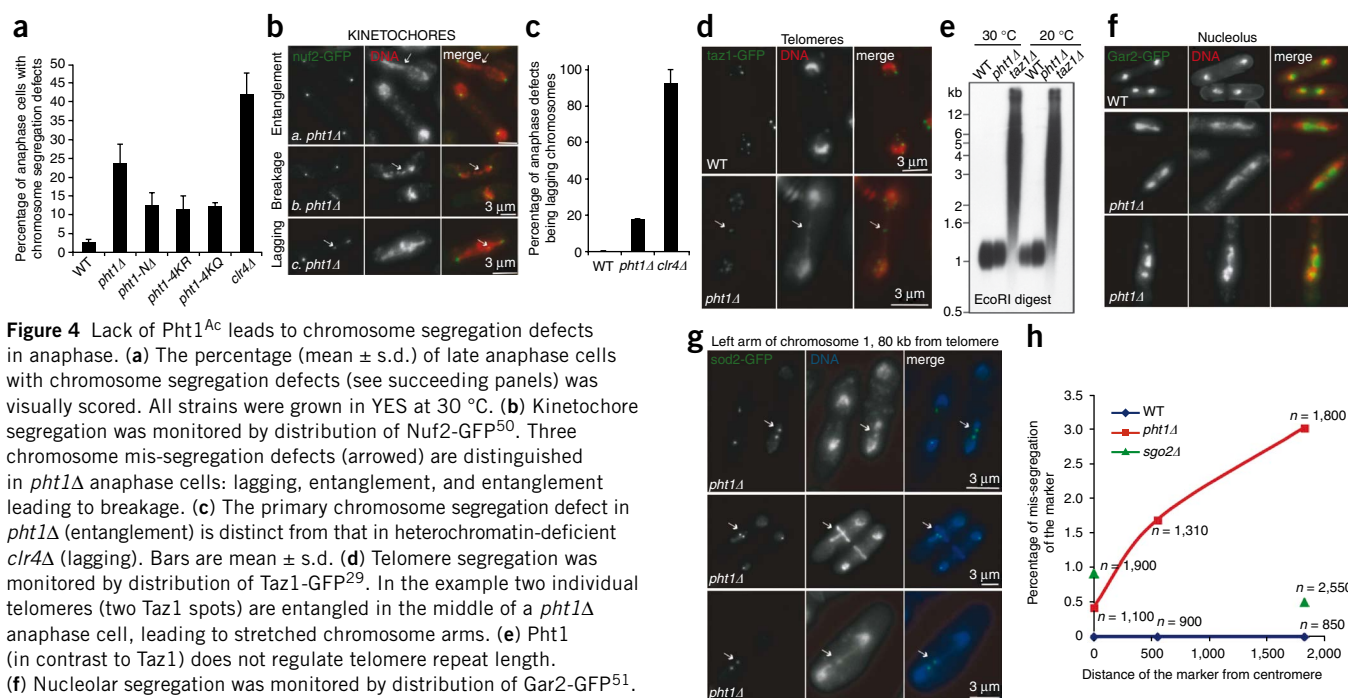
Figure 4 Lack of Pht1[Ac] leads to chromosome segregation defects in anaphase. (**a**) The percentage (mean ± s.d.) of late anaphase cells with chromosome segregation defects (see succeeding panels) was visually scored. All strains were grown in YES at 30 °C. (**b**) Kinetochore segregation was monitored by distribution of Nuf2-GFP[50]. Three chromosome mis-segregation defects (arrowed) are distinguished in *pht1Δ* anaphase cells: lagging, entanglement, and entanglement leading to breakage. (**c**) The primary chromosome segregation defect in *pht1Δ* (entanglement) is distinct from that in heterochromatin-deficient *clr4Δ* (lagging). Bars are mean ± s.d. (**d**) Telomere segregation was monitored by distribution of Taz1-GFP[29]. In the example two individual telomeres (two Taz1 spots) are entangled in the middle of a *pht1Δ* anaphase cell, leading to stretched chromosome arms. (**e**) Pht1 (in contrast to Taz1) does not regulate telomere repeat length. (**f**) Nucleolar segregation was monitored by distribution of Gar2-GFP[51]. In many *pht1Δ* cells the nucleolus appears stretched or fragmented. (**g,h**) Chromosome marker loss in *pht1Δ* cells increases with distance from the centromere. GFP-marked loci locations (*cen2-lacO*, 5 kb from CEN2; *ade3-lacO*, 1,350 kb from TEL1-I; *sod2-lacO*, 80 kb from TEL1-I (ref. 30)) were used to monitor and quantify chromosome segregation defects. *n* represents the number of binucleate cells counted for each marker in each background.

and chromosome segregation and/or cytokinesis (for example, *cut8*, DASH complex) (**Fig. 3f**). These are reminiscent of the synthetic interactions displayed by *Sc htz1Δ*[15,17], further suggesting that there is strong conservation of H2A.Z function in each organism.

Chromosome loss in pht1Δ is caused by entanglement at anaphase

Knockout or depletion of H2A.Z in *Sc*[15] or mammalian cells[5] leads to increased rates of chromosome loss. This phenotype was also observed if any component of the *Sp* Pht1[Ac] pathway was disrupted, including mutants in *swr1* (and *msc1*), *pht1* (*pht1Δ*, *-4KR* or *-4KQ*) or *mst1* (refs. 16,25,26) (**Supplementary Table 2**). One possible explanation for chromosome instability is disruption of the centromere[27]. However, as in *htz1Δ* cells[9], centromere structure and function appeared normal in *pht1* cells (**Supplementary Fig. 1**).

Cytological analysis of individual *Sp* cells revealed a more than eight-fold increase (relative to wild type (WT)) in the number of *pht1Δ* cells with anaphase chromosome segregation defects (**Fig. 4a**). Three specific categories of anaphase defects were distinguished using the kinetochore marker Nuf2-GFP: (i) lagging chromosomes, in which the mis-segregating chromatin contains at least one kinetochore; (ii) chromosome entanglement, in which the mis-segregating chromatin is stretched between the spindle poles but contains no kinetochore; and (iii) entanglement leading to breakage, in which broken pieces of chromatin with no kinetochore lag on the spindle (**Fig. 4b**). The primary segregation defect in *pht1Δ* cells was entanglement (>80% of defective anaphases). This was clearly distinct from the primary anaphase segregation defect in heterochromatin-deficient *clr4Δ* cells (>90% lagging chromosomes) (**Fig. 4c**). Lagging chromosomes result from merotely, a defect in which a single kinetochore attaches to microtubules emanating from opposite spindle poles[28]. Thus, to a large extent, kinetochore-microtubule attachments appear normal in *pht1* cells, supporting our observation from chromatin immunoprecipitation (ChIP)

studies of a WT-like centromere in *pht1* mutants (**Supplementary Fig. 1c**). Consistent with this result, *pht1* cells did not activate the spindle checkpoint, nor did they rely on spindle-checkpoint genes for survival (data not shown).

Chromosome entanglement in *pht1* cells was particularly obvious when we followed telomere segregation at anaphase. To do so, we used the telomere-binding protein Taz1-GFP as a marker. In a normal mitosis, six Taz1-GFP spots (identifying the left and right telomeres on the three *Sp* chromosomes) migrate to opposite poles with the bulk of DNA. However, in *pht1* cells we often observed two or more Taz1-GFP foci entangled in the center, leading to stretched chromosome arms (**Fig. 4d**). One possible explanation for this entanglement is a defect in telomere function comparable to that observed in cells lacking the protection factor Taz1 (ref. 29). However, many of the phenotypes of *taz1Δ* were not shared by *pht1Δ*: for example, cold sensitivity, size of the chromatin bridge, presence of Rad22 foci, and *rqh1-SM* suppression (**Supplementary Fig. 2**). In addition, and most noteworthy, although telomere-repeat length was greatly increased in *taz1Δ*, it was comparable to WT in *pht1Δ* (**Fig. 4e**).

To quantify how frequently the entanglement in *pht1* cells leads to chromosome loss, we employed a series of strains containing: (i) lacOperator (*lacO*) repeats integrated at different chromosomal locations, and (ii) LacI-GFP, the fluorophore-marked *lacO* binding protein[30]. Unexpectedly, marker loss in mitotic *pht1Δ* cells increased with distance from the centromere, suggesting that they generally lost broken pieces of chromosomes rather than whole chromatids (**Figs. 4f–h**). This is in sharp contrast to *sgo2Δ* cells, which are unable to correct chromosome biorientation defects[31,32]. In *sgo2Δ* cells marker loss was similar irrespective of chromosome position, suggesting the loss of whole chromatids (**Fig. 4h**). Together these observations suggest that the primary role of Pht1 in chromosome transmission is to maintain overall chromosome architecture rather than to regulate the function of a specific region (such as the centromere or telomere).

Figure 5 Pht1 plays a role in chromosome architecture and compaction. (**a**) *pht1Δ* (and *-4KR* or *-4KQ*; not shown) cells frequently lose the 'arrowhead' structure of segregating chromosomes in anaphase, indicating a disruption of chromatin architecture (mean ± s.d.). In the example, each anaphase (WT and *pht1Δ*) is at roughly the same stage, 6.5 μm between the poles. (**b**) The chromosome segregation defects of *pht1Δ*, but not *taz1Δ*, can be rescued by chromosome hypercondensation induced by prolonged mitotic arrest. WT, *pht1Δ* or *taz1Δ* cells in the background of Nda3 (blue) or a cold-sensitive tubulin mutant *nda3-KM311* (red) were placed at the restrictive temperature (20 °C, 6 h), where *nda3-KM311* failed to assemble microtubules and underwent spindle-dependent checkpoint arrest. Cells were released into anaphase at the permissive temperature (32 °C) and scored for chromosome segregation defects. Arresting with HU had no effect on the phenotype. (**c**) *pht1Δ* partially rescued mutants in three subunits of condensin (each SMC and the kleisin: *cut3-477*, *cut14-208* and *cnd2-1*), but is synthetic with a mutant in *cohesin* (kleisin: *rad21-K1*). The ability to rescue *condensin* was not shared by deletions of the Set1 methyltransferase or Gcn5 acetyltransferase. Spot tests were ten-fold dilutions onto YES plates. (**d**) WT or *pht1Δ* (additionally containing Cut3.HA₃ and *cdc25-22*) were arrested in

G₂ and released into the cell cycle (with samples taken every 25 min as in Online Methods). Septation index confirmed that each population completed mitosis by 125 min (peak septation, shaded in gray). ChIP was used to monitor condensin and H3K9me2 at various locations, including the Chr I centromere (for primer schematic see **Supplementary Fig. 1c**) and rDNA. Whereas H3K9 dimethylation at *imr1* and *otr1* followed similar kinetics in WT and *pht1Δ*, Cut3.HA₃ dropped prematurely at all locations in the absence of the histone variant (see also **Supplementary Fig. 3d**). "Relative fold enrichment" in the ChIP quantitation graphs is the ratio between the specific signal at each location and the respective input.
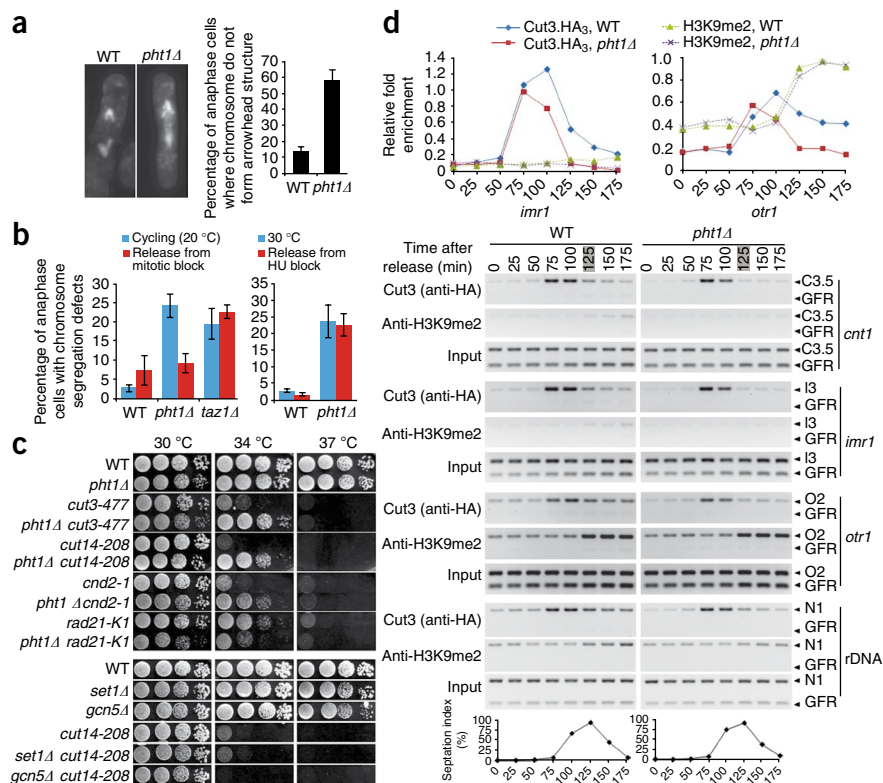
Pht1 has a role in chromosome architecture and/or compaction

Chromosomes condense to a folded rod-shaped structure upon mitotic entry. As the chromatids are pulled to the spindle poles in early anaphase, the chromosome arms trail behind the centromeres, forming a distinctive 'arrowhead' structure. This was lost in > 50% of cells lacking *pht1* (**Fig. 5a**). The occurrence of such a generalized defect further supports the idea that Pht1 regulates overall chromosome architecture rather than that of specific loci.

The primary chromosome segregation defect in *pht1* cells, chromosome entanglement despite accurate centromere segregation (**Fig. 4**), is reminiscent of that observed in mutants of condensin, a five-subunit complex instrumental to the architecture and segregation of chromosomes in mitosis[33–36] (**Supplementary Fig. 3a**). We thus speculated that *pht1* mutants may misregulate chromosome condensation during anaphase. If so, it may be possible to suppress their defect by forcing chromosome hypercondensation. To this end we used the cold-sensitive tubulin mutant, *nda3-KM311*, that fails to assemble microtubules at the restrictive temperature (20 °C), leading to a spindle-dependent checkpoint arrest[37]. This prolonged early mitotic arrest induces chromosome hypercondensation[37], and when shifted to the permissive temperature (32 °C) these cells enter a synchronous anaphase[31,37]. This prolonged mitotic arrest specifically rescued the chromosome segregation defect of *pht1Δ* but not *taz1* cells (**Fig. 5b**). Arresting *pht1Δ* cells in S-phase with hydroxyurea (HU), which depletes nucleotide pools, had no effect on the chromosome segregation defect, showing that merely prolonging the cell cycle was not sufficient to rescue *pht1* defects (**Fig. 5b**).

A functional relationship would be indicated by genetic interaction, so we tested for that between *pht1* and *condensin*. Unacetylatable *pht1* or *pht1* each raised the restrictive temperature of *ts* alleles of three complex subunits: *cut3-477* (*smc4-S1147P*), *cut14-208* (*smc2-S861P*) and *cnd2-1* (*cnd2-A114T*) (**Fig. 5c** and **Supplementary Fig. 3b**). This partial rescue was specific, as *pht1* was synthetic with *rad21-K1*, a mutant in the condensin-related complex cohesin, which holds sister chromatids together before anaphase onset. This suppression is unlikely to be mediated through indirect transcriptional effects (for example, increased expression of condensin) because the mRNA levels (as determined by gene expression microarray) of all tested complex subunits and known regulators (for example, Cut17, Ark1, Top2, Fin1, Pim1, Pic1, Acr1, Nuc1) in WT cells were comparable to those in *pht1Δ* and unacetylatable *pht1* cells (**Supplementary Fig. 3c** and data not shown). In addition, the partial rescue was not observed with deletion of two other transcriptional regulators: the Set1 methyltransferase or Gcn5 acetyltransferase (**Fig. 5c**).

Our results are consistent with a model where an acetylated form of Pht1 regulates condensin loading and/or localization in mitosis. To test this, we arrested WT or *pht1* cells expressing Cut3 C-terminally tagged with the hemagglutinin YPYDVPDYA peptide (Cut3.HA₃) at the G₂-M boundary, and then monitored condensin occupancy kinetics through a synchronous mitosis (**Fig. 5d**). To first ensure that mitotic progression in WT and *pht1Δ* cells followed similar kinetics, we examined the peak septation index and H3K9me2 in each population. A newly formed septum indicates the completion of mitosis and can be visualized by specific staining with Calcofluor (see Online Methods). H3K9me2 is markedly reduced at centromeric repeats (*otr*) during mitosis, increasing as cells enter G₁/S[38]. Each

Figure 6 H2A.Z plays a role in higher-order chromosome architecture. (**a**). Upper row: the localization and association of condensin with chromosomes is tightly regulated. The complex is primarily (but not exclusively) found in the cytoplasm through interphase, and imported into the nucleus at prophase for chromosome loading, with levels peaking at anaphase[52,53]. Lower row: the pathway in *H2A.ZΔ* cells. Condensin loads normally but prematurely dissociates (**Fig. 5d**). This explains the poorly resolved structure observed in anaphase (**Fig. 5a**), which likely leads to chromosome entanglement and loss (**Fig. 4**). (**b**) Sister chromatids in condensin mutants are 'fuzzy' and resolve poorly at prophase. The sisters remain connected by chromatin bridges as they pull apart in anaphase (see **Supplementary Fig. 3a**). (**c**) The rescue by *pht1Δ* (and unacetylatable mutants) of various chromosome architecture mutants (*condensin* and Topo II; **Fig. 5c** and **Supplementary Figs. 3b** and **4**) indicates that a partially compensatory condensed topology exists in *pht1Δ* cells. (**d**) Model separates mitotic chromosome condensation and architecture into two stages: initial compaction and maintenance. The first stage is dependent on the poorly characterized activity (or factor) RCA; the second, on the condensin complex and topoisomerase II. H2A.Z may have a dual regulatory role: somehow opposing RCA, yet stabilizing the association of condensin with chromatin.

pattern was indistinguishable between WT and *pht1Δ* cells (**Fig. 5d**). When we examined condensin recruitment, Cut3.HA$_3$ initially (≤75 min) followed similar kinetics at the centromere (*cnt*, *imr* and *otr*) and ribosomal DNA of WT and *pht1Δ* cells (**Fig. 5d** and **Supplementary Fig. 3d**). However, significant differences were then observed: Cut3.HA$_3$ levels continued to increase in WT cells, peaking at 100 min before dropping at 125 min (the latter corresponding to the peak septation index time point; **Fig. 5d**). However, in *pht1Δ* condensin delocalization began by 100 min, indicating the premature dissociation of the complex from chromatin. This likely explains many of our observations in these cells: loss of the anaphase arrowhead structure leading to chromosome entanglement and the loss of telomere-proximal regions (**Fig. 5**).

DISCUSSION

In this work we identify and characterize a previously unknown role for the histone variant H2A.Z (*Sp* Pht1) in chromosome architecture at anaphase. In the absence of Pht1, chromosomes frequently entangle in anaphase, which can lead to breakage and loss, particularly of telomere-proximal regions. We provide evidence that chromosome entanglement in *pht1Δ* is most likely due to premature dissociation of the condensin complex in anaphase. We also demonstrate that the factors involved in the chromatin loading and acetylation of H2A.Z are highly conserved in *Sc* and *Sp*. The last common predecessor of these yeasts was ~380 million years ago (mya)[39]; by comparison, the last common predecessor of the entire mammalian class existed ~165 mya[40], whereas the primate line split to humans and gorillas ~8 mya[41].
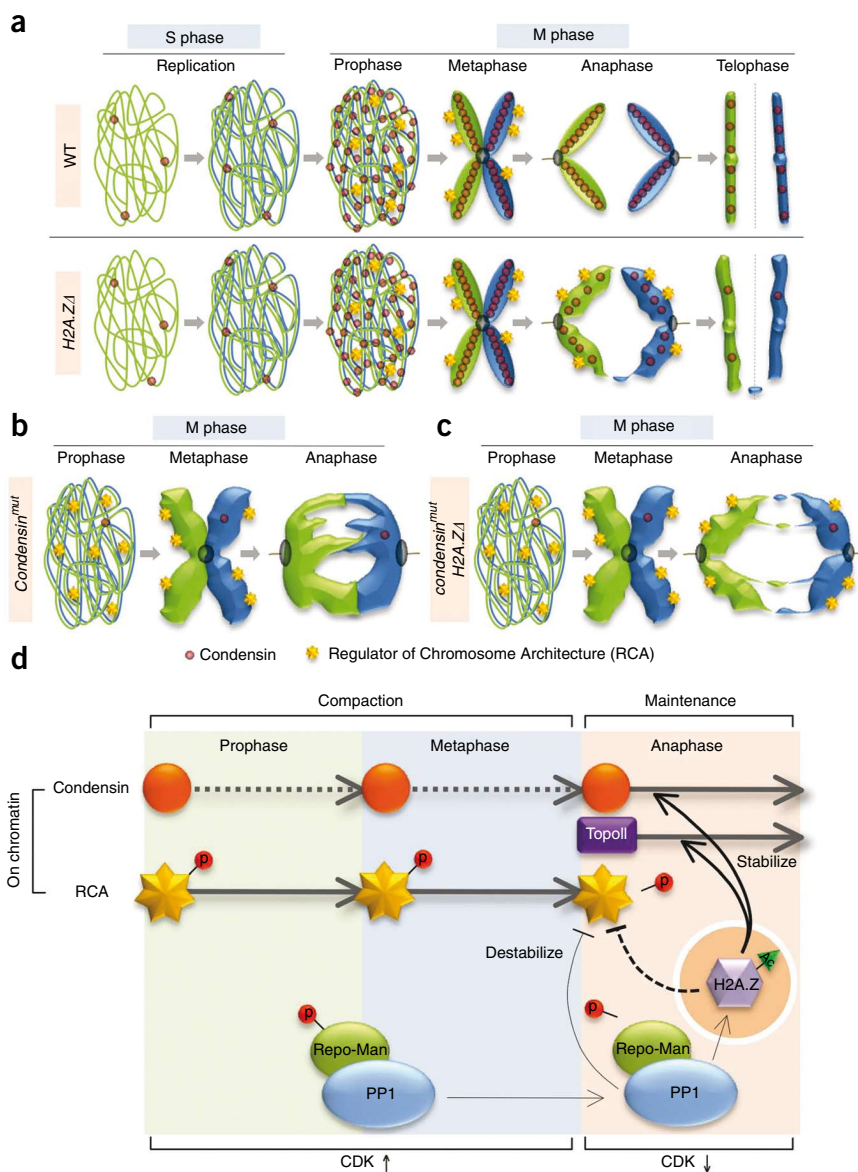
We propose that because the pathways regulating H2A.Z localization, modification and function are so well conserved, the role of the histone variant in chromosome architecture will be equally widespread.

Extensive conservation of the SWR-C

Comprehensive proteomic analyses identify two subunits in the *Sp* SWR-C not seen in its *Sc* counterparts Msc1 and SPAC4H3.02c (ref. 42) (**Fig. 2a** and **Supplementary Table 1**). Both deletions are epistatic with *pht1* (ref. 20) (**Fig. 3c**), further suggesting a functional relationship. Msc1 was originally identified as a multicopy suppressor of cells defective for checkpoint kinase Chk1 (Rad27) function[43]. Recent work has found an epistatic chromosome loss phenotype in *pht1Δ* and *msc1Δ*, and has suggested that Msc1 is upstream of Pht1 in this pathway[26], a relationship our data supports (for example, **Fig. 2c**). Msc1 was recently shown to interact with the Mst1 acetyltransferase by yeast two-hybrid analysis[16]. Despite this, any physical interaction between Mst1 and Msc1 is likely to be transient, as Msc1.TAP purification did not identify Mst1 (or any nonshared subunit of the Swr1 and Mst1 complexes; **Supplementary Table 1**), and unique members of the Mst1-C do not copurify Msc1 (data not shown). However, the

link between the Swr1 and Mst1 complexes is interesting, and may suggest that Msc1 directly recruits Mst1 to sites of Pht1 integration.

N-terminal acetylation is integral to Pht1 function

The SWR-C is required for the assembly of Pht1 into chromatin, where it is acetylated by Mst1 (**Figs. 1** and **2**). This relationship between the ATPase (Swr1), histone variant (H2A.Z) and KAT5-family acetyltransferase (Mst1) appears to be widely conserved[9,15,44–47]. Unacetylatable *pht1* phenocopies *pht1Δ* throughout this work but is perhaps most noteworthy in large-scale gene expression and genetic analyses (**Fig. 3**). This strongly suggests that acetylation of the histone is integral to its function. Based on *Sc* Htz1, it is likely that all four lysine residues in the Pht1 N terminus are modified[10,11]. However, our Pht1[Ac] antibody was raised to a tetra-acetylated peptide (**Fig. 1a**), and the unacetylatable *pht1* used throughout this work has mutations at all four N-terminal lysines, so these individual modifications are as yet unconfirmed. *mst1*-L271P reduces Pht1[Ac] below the threshold of detection (**Fig. 1d**), which suggests that we have identified the major enzyme for this modification. In this regard, we note that *mst1* mutants also show increased rates of chromosome loss[16], likely due in part to reduced Pht1[Ac].

Pht1 regulates chromosome architecture at anaphase

Knockout or depletion of H2A.Z in *Sc*[15], *Sp*[25,26] or mammalian cells[5] leads to increased rates of chromosome loss. An acetylated form of H2A.Z mediates chromosome stability role in both *Sc*[9] and *Sp* (this work), strongly suggesting that this will prove to be the case in other organisms. Directly monitoring chromosome segregation in individual *Sp* cells allowed us to show that lack of Pht1 induces chromosome arm entanglements in anaphase that can lead to chromosome breaks (**Fig. 4**). Furthermore, Pht1 is required for the stable association of condensin with chromatin through anaphase (**Fig. 5d**), and the chromosome entanglement in *pht1Δ* cells can be rescued by a pre-anaphase arrest where chromosomes hypercondense (**Fig. 5b**). Thus, the lack of Pht1 interferes with chromosome architecture in anaphase. However, it also improves the viability of mutants that regulate this process, such as those in condensin (*cut3-477*, *cut14-208*, *cnd2-1*) or topoisomerase II (*top2-191*) (**Fig. 5c** and **Supplementary Fig. 4**). To resolve this apparent contradiction, we propose that Pht1 actually plays a dual role in mitotic chromosome architecture (see below and **Fig. 6**).

Mitotic defects in a chicken condensin mutant primarily occur in anaphase: chromosomes prematurely lose their compact organization as they move to the poles[48]. Thereafter, individual chromatids can no longer be distinguished and prominent chromatin bridges are visible in >90% of cells (for example, **Fig. 6b** and **Supplementary Fig. 3a**). These phenotypes can be overcome if Repo-Man, a targeting subunit for protein phosphatase 1 (PP1), is unable to direct the phosphatase to chromosomes in anaphase[48]. In WT cells Repo-Man is subject to CDK-dependent phosphorylation(s) to abrogate chromosome binding at early mitosis when CDK levels are high. Chromosome compaction at this stage is only slightly affected in condensin mutants, prompting the proposal that an as-yet-uncharacterized activity, regulator of chromosome architecture (RCA), drives initial condensation. RCA is then inhibited in a process dependent on Repo-Man and PP1 after CDK levels fall at anaphase onset and condensin steps in to stabilize chromosome architecture until mitosis completes[48] (all modeled in **Fig. 6d**).

The above model suggests that there are at least two steps in chromosome condensation. The first is RCA-dependent compaction to the characteristic X-shaped mitotic chromosome. The second is the condensin-dependent maintenance of a robust architecture that can withstand the pulling forces of microtubules in anaphase. Our data suggests that Pht1 regulates both steps: promoting the inhibition of RCA and stabilizing the association of condensin. As above, artificial maintenance of RCA activity in anaphase by preventing the loading of PP1 to chromatin partly rescues the chromosome segregation defects of chicken *smc2* mutants[48]. This is reminiscent of the genetic interactions between *pht1* and *condensin* (for example, **Fig. 5c**). It is highly likely that RCA is conserved in *Sp*, as deletion of the fission yeast PP1 ortholog that localizes on chromatin (PP1[Dis2]), also partly rescues *cut3-477* (**Supplementary Fig. 4b**). Finally, we have recently shown that *Sc* Bud14, a regulator of *Sc* PP1 (Glc7), is required for the efficient loading of Htz1 onto chromatin (and subsequent acetylation of the histone variant)[49]. This suggests that H2A.Z could act downstream of PP1 to inhibit RCA in anaphase (**Fig. 6d**). Further studies are underway to test this model.

METHODS

Methods and any associated references are available in the online version of the paper at http://www.nature.com/nsmb/.

1. Henikoff, S., Furuyama, T. & Ahmad, K. Histone variants, nucleosome assembly and epigenetic inheritance. *Trends Genet.* **20**, 320–326 (2005).
2. Latham, J.A. & Dent, S.Y.R. Cross-regulation of histone modifications. *Nat. Struct. Mol. Biol.* **14**, 1017–1024 (2007).
3. Millar, C.B. & Grunstein, M. Genome-wide patterns of histone modifications in yeast. *Nat. Rev. Mol. Cell Biol.* **7**, 657–666 (2006).
4. Faast, R. *et al.* Histone variant H2A.Z is required for early mammalian development. *Curr. Biol.* **11**, 1183–1187 (2001).
5. Rangasamy, D., Greaves, I. & Tremethick, D.J. RNA interference demonstrates a novel role for H2A.Z in chromosome segregation. *Nat. Struct. Mol. Biol.* **11**, 650–655 (2004).

6. Leach, T.J. *et al.* Histone H2A.Z is widely but non-randomly distributed in chromosomes of *Drosophila melanogaster*. *J. Biol. Chem.* **275**, 23267–23272 (2000).

7. Rangasamy, D., Berven, L., Ridgway, P. & Tremethick, D.J. Pericentric heterochromatin becomes enriched with H2A.Z during early mammalian development. *EMBO J.* **22**, 1599–1607 (2003).

8. Greaves, I.K., Rangasamy, D., Devoy, M., Marshall Graves, J.A. & Tremethick, D.J. The X and Y chromosomes assemble into H2A.Z, containing facultative heterochromatin, following meiosis. *Mol. Cell. Biol.* **26**, 5394–5405 (2006).

9. Keogh, M.-C. The *Saccharomyces cerevisiae* histone H2A variant Htz1 is acetylated by NuA4. *Genes Dev.* **20**, 660–665 (2006).

10. Millar, C.B., Xu, F., Zhang, K. & Grunstein, M. Acetylation of H2AZ lysine 14 is associated with genome-wide gene activity in yeast. *Genes Dev.* **20**, 711–722 (2006).

11. Babiarz, J.E., Halley, J.E. & Rine, J. Telomeric heterochromatin boundaries require NuA4-dependent acetylation of histone variant H2A.Z in *Saccharomyces cerevisiae*. *Genes Dev.* **20**, 700–710 (2006).

12. Ren, Q. & Gorovsky, M.A. Histone H2A.Z acetylation modulates an essential charge patch. *Mol. Cell* **7**, 1329–1335 (2001).

13. Bruce, K. *et al.* The replacement histone H2A.Z in a hyperacetylated form is a feature of active genes in the chicken. *Nucleic Acids Res.* **33**, 5633–5639 (2005).

14. Bonenfant, D., Coulot, M., Towbin, H., Schindler, P. & van Oostrum, J. Characterization of histone H2A and H2B variants and their post-translational modifications by mass spectrometry. *Mol. Cell. Proteomics* **5**, 541–552 (2006).

15. Krogan, N.J. *et al.* Regulation of chromosome stability by the histone H2A variant Htz1, the Swr1 chromatin remodeling complex and the histone acetyltransferase NuA4. *Proc. Natl. Acad. Sci. USA* **101**, 13513–13518 (2004).

16. Gómez, E.B., Nugent, R.L., Laria, S. & Forsburg, S.L. *S. pombe* histone acetyltransferase Mst1 (KAT5) is an essential protein required for damage response and chromosome segregation. *Genetics* **179**, 757–771 (2008).

17. Krogan, N.J. *et al.* A Snf2-Family ATPase complex required for recruitment of the histone H2A variant Htz1. *Mol. Cell* **12**, 1565–1576 (2003).

18. Kobor, M.S. *et al.* A protein complex containing the conserved Swi2/Snf2-related ATPase Swr1p deposits histone variant H2A.Z into euchromatin. *PLoS Biol.* **2**, e131 (2004).

19. Mizuguchi, G. *et al.* ATP-driven exchange of histone H2AZ variant catalyzed by SWR1 chromatin remodeling complex. *Science* **303**, 343–348 (2004).

20. Roguev, A. *et al.* Conservation and rewiring of functional modules revealed by an epistasis map (E-MAP) in fission yeast. *Science* **322**, 405–410 (2008).

21. Roguev, A., Wiren, M., Weissman, J.S. & Krogan, N.J. High-throughput genetic interaction mapping in the fission yeast *Schizosaccharomyces pombe*. *Nat. Methods* **4**, 861–866 (2007).

22. Schuldiner, M. *et al.* Exploration of the function and organization of the yeast early secretory pathway through an epistatic miniarray profile. *Cell* **123**, 507–519 (2005).

23. Collins, S.R. *et al.* Functional dissection of protein complexes involved in yeast chromosome biology using a genetic interaction map. *Nature* **446**, 806–810 (2007).

24. Collins, S.R., Schuldiner, M., Krogan, N.J. & Weissman, J.S. A strategy for extracting and analyzing large-scale quantitative epistatic interaction data. *Genome Biol.* **7**, R63 (2006).

25. Carr, A.M. *et al.* Analysis of a histone H2A variant from fission yeast: evidence for a role in chromosome stability. *Mol. Gen. Genet.* **245**, 628–635 (1994).

26. Ahmed, S., Dul, B., Qiu, X. & Walworth, N.C. Msc1 acts through histone H2A.Z to promote chromosome stability in *Schizosaccharomyces pombe*. *Genetics* **177**, 1487–1497 (2008).

27. Ekwall, K. Epigenetic control of centromere behaviour. *Annu. Rev. Genet.* **41**, 63–81 (2007).

28. Gregan, J. *et al.* The kinetochore proteins Pcs1 and Mde4 and heterochromatin are required to prevent merotelic orientation. *Curr. Biol.* **17**, 1190–1200 (2008).

29. Cooper, J.P., Nimmo, E.R., Allshire, R.C. & Cech, T.R. Regulation of telomere length and function by a Myb-domain protein in fission yeast. *Nature* **385**, 744–747 (1997).

30. Ding, D.-Q., Yamamoto, A., Haraguchi, T. & Hiraoka, Y. Dynamics of homologous chromosome pairing during meiotic prophase in fission yeast. *Dev. Cell* **6**, 329–341 (2004).

31. Vanoosthuyse, V., Prykhozhij, S. & Hardwick, K.G. Shugoshin 2 regulates localization of the chromosomal passenger proteins in fission yeast mitosis. *Mol. Biol. Cell* **18**, 1657–1669 (2007).

32. Kawashima, S.A. *et al.* Shugoshin enables tension-generating attachment of kinetochores by loading Aurora to centromeres. *Genes Dev.* **21**, 420–435 (2007).

33. Nakazawa, N. *et al.* Dissection of the essential steps for condensin accumulation at kinetochores and rDNAs during fission yeast mitosis. *J. Cell Biol.* **180**, 1115–1131 (2008).

34. Saka, Y. *et al.* Fission yeast cut3 and cut14, members of a ubiquitous protein family, are required for chromosome condensation and segregation in mitosis. *EMBO J.* **13**, 4938–4952 (1994).

35. Sutani, T. *et al.* Fission yeast condensin complex: essential roles of non-SMC subunits for condensation and Cdc2 phosphorylation of Cut3/SMC4. *Genes Dev.* **13**, 2271–2283 (1999).

36. Hagstrom, K.A., Holmes, V.F., Cozzarelli, N.R. & Meyer, B.J. *C. elegans* condensin promotes mitotic chromosome architecture, centromere organization, and sister chromatid segregation during mitosis and meiosis. *Genes Dev.* **16**, 729–742 (2002).

37. Hiraoka, Y., Toda, T. & Yanagida, M. The NDA3 gene of fission yeast encodes β-tubulin: a cold-sensitive nda3 mutation reversibly blocks spindle formation and chromosome movement in mitosis. *Cell* **39**, 349–358 (1984).

38. Chen, E.S. *et al.* Cell cycle control of centromeric repeat transcription and heterochromatin assembly. *Nature* **451**, 734–737 (2008).

39. Sipiczki, M. Where does fission yeast sit on the tree of life? *Genome Biol.* **1**, 1011 (2000).

40. O'Brien, S.J. *et al.* The promise of comparative genomics in mammals. *Science* **286**, 458–462 (1999).

41. Takahata, N. & Satta, Y. Evolution of the primate lineage leading to modern humans: phylogenetic and demographic inferences from DNA sequences. *Proc. Natl. Acad. Sci. USA* **94**, 4811–4815 (1997).

42. Shevchenko, A. *et al.* Chromatin central: towards the comparative proteome by accurate mapping of the yeast proteomic environment. *Genome Biol.* **9**, R167 (2008).

43. Ahmed, S., Palermo, C., Wan, S. & Walworth, N.C. A novel protein with similarities to Rb binding protein 2 compensates for loss of *chk1* function and affects histone modification in fission yeast. *Mol. Cell. Biol.* **24**, 3660–3669 (2004).

44. Choi, K. *et al. Arabidopsis* homologs of components of the SWR1 complex regulate flowering and plant development. *Development* **134**, 1931–1941 (2007).

45. Ruhl, D.D. *et al.* Purification of a human SCRAP complex that remodels chromatin by incorporating the histone variant H2A.Z into nucleosomes. *Biochemistry* **45**, 5671–5677 (2006).

46. Kusch, T. *et al.* Acetylation by Tip60 is required for selective histone variant exchange at DNA lesions. *Science* **306**, 2084–2087 (2004).

47. Updike, D.L. & Mango, S.E. Temporal regulation of foregut development by HTZ-1/H2A.Z and PHA-4/FoxA. *PLoS Genet.* **2**, e161 (2006).

48. Vagnarelli, P. *et al.* Condensin and Repo-Man-PP1 co-operate in the regulation of chromosome architecture during mitosis. *Nat. Cell Biol.* **8**, 1133–1142 (2006).

49. Fiedler, D. *et al.* Functional organization of the *S. cerevisiae* phosphorylation network. *Cell* **136**, 952–963 (2009).

50. Nabetani, A., Koujin, T., Tsutsumi, C., Haraguchi, T. & Hiraoka, Y. A conserved protein, Nuf2, is implicated in connecting the centromere to the spindle during chromosome segregation: a link between the kinetochore function and the spindle checkpoint. *Chromosoma* **110**, 322–334 (2001).

51. Gulli, M.P. *et al.* gar2 is a nucleolar protein from *Schizosaccharomyces pombe* required for 18S rRNA and 40S ribosomal subunit accumulation. *Nucleic Acids Res.* **23**, 1912–1918 (1995).

52. Hagstrom, K.A. & Meyer, B.J. Condensin and cohesin: more than chromosome compactor and glue. *Nat. Rev. Genet.* **4**, 520–534 (2003).

53. Hirano, T. Condensins: Organizing and segregating the genome. *Curr. Biol.* **15**, R265–R275 (2005).

ONLINE METHODS

Materials. Antibodies, strains and oligos are listed in **Supplementary Tables 3–5**, respectively. Peroxidase anti-peroxidase (antiPAP) to recognize the TAP tag in immunoblotting was obtained from Sigma. Rabbit polyclonal affinity-purified anti-*Sp* H2A.Z antibodies were from Active Motif. C-terminal anti-Pht1 (no. 39640) was raised against residues 121–134 (C-KQLLIRTKEKYPEE), anti-Pht1[Ac] (no. 39642) against residues 1–20 (SGGG[K^{Ac}]G[K^{Ac}]HVGG [K^{Ac}]GGS[K^{Ac}]IGER-C) (**Fig. 1a**). We used the terminal C residue on each peptide to couple to keyhole limpet hemocyanin for immunization or a sulfolink resin for affinity purification.

Cell fractionation. *Sp* cell fractionations were performed essentially as described for *Sc*[9], with cultures harvested at OD$_{600}$ ~0.5. Total, cytoplasmic, nuclear and chromatin fractions were analyzed by SDS-PAGE and immunoblotting.

Cell-cycle synchronization: ChIP and septation analyses. Cell-cycle synchronization by *cdc25-22* was as previously described[33,54]. Briefly, cultures were G$_2$-arrested at the nonpermissive temperature (36.5 °C, 4.5 h) before synchronized release at 24.5 °C. Aliquots were collected at 25-min intervals and fixed either with formaldehyde for ChIP (50 ml) or in 70% (v/v) ethanol for cell-septation analysis (500 µl). The latter were collected by flash spin centrifugation at 10,000 rpm (Eppendorf 5810R with microfuge rotor F45-30-11), washed in PBS, and resuspended in PBS + Calcofluor (25 µg ml^{-1}). Septum formation was determined by microscopy under UV excitation with >300 cells counted per time point.

Gene expression microarrays. Total RNA was isolated using a hot-phenol protocol[55]. 10–20 µg of total RNA were labeled by direct incorporation of either Cy3- or Cy5-dCTP (GE Healthcare), and the fluorescently labeled product was hybridized to *Sp* cDNA microarrays[55]. Microarrays were scanned with a GenePix 4000B laser scanner (Axon Instruments), fluorescence-intensity ratios were calculated with GenePix Pro (Axon Instruments) and data were normalized using a previously described script[55]. At least three biological repeats were analyzed for each mutant with dye swaps. To analyze the data, repeats for every given mutant were averaged. The significance of overlaps between different gene lists was calculated in GeneSpring (Agilent) using a standard Fisher's exact test, and *P* values adjusted with a Bonferroni multiple testing correction.

Microscopic analysis of mitotic chromosomes. *Sp* cells with green fluorescent protein (GFP)-tagged factors were grown in rich medium and briefly (< 30 s) fixed in 100% methanol before observation. DNA was visualized by DAPI staining. Imaging was performed with an Intelligent Imaging Innovations (3i) Marianas system. This uses a Zeiss Axiovert fluorescence microscope, a CoolSNAP HQ charge-coupled device camera (Photometrics) and Slidebook software (3i; Photometrics).

Mini-chromosome loss assay. Deletions were mated into a *Ch16* mini-chromosome strain containing episomal *ade6-M216* to complement genomic *ade6-M210* in *trans*[56]. The presence of both alleles results in white colonies; loss of *Ch16* leads to red. Strains from a white colony were patched overnight onto YES, resuspended and dispensed onto plates with limiting adenine to allow optimal color development. Red, white and sectored colonies were counted and chromosome loss rates calculated.

PEM2 analysis. Genetic screening of *pht1* mutants was performed with the PEM-2 system[20,21]. NAT-marked mutant queries in the h$^-$ PEM2 background (p392 (KFP171); **Supplementary Table 4**) were mated against the Bioneer G418-resistant deletion set (h$^+$, *ura4-D18*, *leu1-32*, *ade6-M21X*, *yfg*Δ::KanMX). Mating, haploid selection, data acquisition and analysis were as previously described[20]. Pair correlation coefficients (CCs) to determine the relationship between genetic screens (as in **Figs. 4b,c**) were calculated by the CORREL function (Excel).

Telomere length by Southern blotting. Genomic DNA was isolated by standard glass bead phenol extraction. 20 µg of genomic DNA was digested with EcoRI, resolved on a 1% (w/v) agarose gel, transferred to a Hybond N$^+$ membrane and probed with radiolabeled 500-bp synthetic telomeric repeats (gift from J. Cooper, Cancer Research UK).

TAP purification of protein complexes. Briefly, 8 l of each C-terminally TAP-tagged strain was grown at 30 °C to OD$_{600}$ ~2.5 in YES medium. Cells were washed twice with distilled, deionized water, resuspended in 0.25 volume buffer E (20 mM HEPES, pH 8.0, 350 mM NaCl, 0.1% Tween-20 plus protease inhibitors) and frozen as noodles in liquid nitrogen. Frozen cells were mixed with dry ice, reduced to powder in a coffee grinder, adjusted to 50 ml total volume with buffer E, and lysed using a Biospec BeadBeater homogenizer lysed by agitation with an equal volume of glass beads (7 × 20 s pulses with 3 minutes on ice between bursts). Extracts were clarified by ultracentrifugation in a 70Ti rotor (30 min, 4 °C, 90,000*g*). Supernatants were collected in 50-ml Falcon tubes and directly added to 200 µl IgG-Sepharose (GE Healthcare) equilibrated in buffer E. Sequential affinity purification on IgG-Sepharose and calmodulin-Sepharose (GE Healthcare) was as before[57]. Half of the affinity-purified protein was vacuum concentrated, resolved by SDS-PAGE and silver stained, with gel slices trypsinized and analyzed by MALDI-TOF. The remainder of the pool was analyzed directly by LC-MS as below.

LC-MS. Protein complexes were digested at 37 °C overnight in 50 mM NH$_4$HCO$_3$ (pH 8.5, 1 mM CaCl$_2$) with a 1:30 molar ratio of recombinant proteomics-grade trypsin (Roche Diagnostics). The resulting peptide mixtures were dried with a SpeedVac (Savant) and reconstituted in 30 µl buffer A (5% v/v acetonitrile, 0.1% v/v formic acid). Peptides were directly loaded from a 96-well microplate autosampler using the EASY-nLC system (Proxeon Biosystems) at 3 µl min^{-1} to a 3 cm precolumn (150 µm i.d.) containing a Kasil frit packed with 5µ Magic C18 100 Å reversed-phase material (Michrom Bioresources). The precolumn was connected via a titanium micro-tee splitter fitted with an electrode for voltage application (2.3 kV) in a vented column set-up to an 8-cm fused silica micro-capillary analytical column (75 µm i.d.) with a homemade laser-pulled spray tip packed with 5µ Magic C18 100 Å reversed-phase resin. For the peptide separation on the analytical column, a water-acetonitrile gradient was applied at an effective flow rate of 400 nl min^{-1}, controlled by the EASY-nLC using a 2-h gradient. All samples were analyzed on an LTQ-Orbitrap XL. The instrument method consisted of one MS full scan (400–1,800 *m/z*) in the Orbitrap mass analyzer, an automatic gain control (AGC) target of 500,000 with a maximum ion injection of 500 ms, one microscan at a resolution of 60,000, and use of the preview scan option. Six data-dependent MS/MS scans were performed in the linear ion trap using the three most intense ions at 35% normalized collision energy. The MS and MS/MS scans were obtained in parallel. AGC targets were 10,000 with a maximum ion injection time of 100 ms. A minimum ion intensity of 1,000 was required to trigger an MS/MS spectrum. The dynamic exclusion was applied using a maximum exclusion list of 500 with one repeat count with a repeat duration of 30 s and exclusion duration of 45 s.

Protein identification and data analysis. Raw files were converted to m/zXML using ReAdW and searched by X!Tandem against an *Sp* database containing known contaminants (human keratins and trypsin). Search parameters were as follows: fragment ion mass tolerance of 0.40 Da and a parent ion tolerance of ±10 ppm. Complete tryptic digestion was assumed. No fixed modifications were specified and oxidation of methionine was specified as a variable modification. Only proteins identified with two or more unique peptides and a protein expectation score (log$_e$ ≤ −3) were considered a positive identification, virtually eliminating false positive identifications in the reported dataset.

54. Dunaway, S. & Walworth, N.C. Assaying the DNA damage checkpoint in fission yeast. *Methods* **33**, 260–263 (2004).
55. Lyne, R. *et al.* Whole-genome microarrays of fission yeast: characteristics, accuracy, reproducibility, and processing of array data. *BMC Genomics* **4**, 27 (2003).
56. Niwa, O., Matsumoto, T. & Yanagida, M. Construction of a mini-chromosome by deletion and its mitotic and meiotic behaviour in fission yeast. *Mol. Genet. Genomics* **203**, 397–405 (1986).
57. Krogan, N.J. *et al.* RNA polymerase II elongation factors of *Saccharomyces cerevisiae*: a targeted proteomics approach. *Mol. Cell. Biol.* **22**, 6979–6992 (2002).

doi:10.1038/nsmb.1688